ISSN 0016-7932, Geomagnetism and Aeronomy, 2023, Vol. 63, No. 4, pp. 473–485. © Pleiades Publishing, Ltd., 2023.
Russian Text © The Author(s), 2023, published in Geomagnetizm i Aeronomiya, 2023, Vol. 63, No. 4, pp. 520–533.

Statistical Studies of Auroral Activity and Perturbations of the Geomagnetic Field at Middle Latitudes

R. Werner[a], V. Guineva[a], I. V. Despirak[b, *], A. A. Lubchich[b], P. V. Setsko[b], A. Atanassov[a], R. Bojilova[c], L. Raykova[a], and D. Valev[a]

[a] *Space Research and Technology Institute, Bulgarian Academy of Sciences, Stara Zagora, 6000 Bulgaria*
[b] *Polar Geophysical Institute, Apatity, Murmansk Oblast, 184209 Russia*
[c] *National Institute of Geophysics, Geodesy and Geography, Bulgarian Academy of Sciences, Sofia, 1113 Bulgaria*
**e-mail: despirak@gmail.com*

Received December 23, 2022; revised March 25, 2023; accepted March 28, 2023

Abstract—In this paper, we statistically analyzed substorm activity at auroral latitudes for 2007–2020 and its relationship with magnetic disturbances at middle latitudes using the INTERMAGNET, SuperMAG, and IMAGE magnetometer data. The appearance and development of magnetic disturbances at auroral latitudes was monitored by the *IL* index (similar to the *AL* index, but according to IMAGE data). For the 2007–2020 period, events that were observed near the meridian of the IMAGE network, in the night sector (2103 MLT), were selected. Two samples of events were used: (1) $IL < -200$ nT for at least 10 min, with an additional criterion for the presence or absence of positive bays at the Panagyurishte station in Bulgaria, and (2) isolated substorms observed on the IMAGE meridian according to the list of Ohtani and Gjerloev (2020). The distributions of the *IL* index, as well as the empirical and theoretical cumulative distribution functions, are obtained, and the of the occurrence of extreme events are also estimated. It is shown that, in general, the *IL* distributions are described well by exponential functions, and out of all events, events accompanied by mid-latitude positive bays were observed in ~65% of cases while their fraction increased with increasing disturbance intensity. Events with positive bays at midlatitudes of MPB and isolated substorms were better described by the Weibull distribution for extreme events. From both distributions, annual and semi-annual variations were identified: annual variations have a summer minimum and a winter maximum, and semi-annual variations have maxima near the equinoxes, which is most likely due to the Russell-McPherron effect. The semi-annual variation is also shown to be more pronounced for events with accompanying mid-latitudinal positive bays.

DOI: 10.1134/S0016793223600303

1. INTRODUCTION

Substorms are known to be associated with the pulsive release of accumulated magnetospheric energy from the magnetotail (e.g., McPherron, 1970; Sergeev et al., 2011). Unlike magnetic storms, the duration of a substorm is, on average, 0.5–2 h. The three-dimensional system of substorm currents is associated with the development of auroral electrojets (eastward and westward) in the ionosphere that are located between the incoming and outgoing currents (Iijima and Potemra 1976; Kamide and Akasofu, 1978). According to ground-based magnetometer data, the development of a magnetic substorm manifests itself as the appearance of negative bays of the horizontal component of the magnetic field at auroral latitudes and positive bays (Mid-latitude Positive Bays or MPBs) at middle latitudes (Akasofu and Meng, 1969; McPherron et al., 1973). In this case, the negative bays correspond to the amplification and movement to the pole of the westward electrojet developing on the night side during the expansion phase of the substorm while the positive bays at mid-latitudes are associated with the development of field-aligned currents of the substorm current wedge, through which the westward electrojet closes to a current break in the plasma sheet of the magnetosphere (McPherron et al., 1978; Kepko et al., 2015).

To describe the intensity of substorm activity, various geomagnetic indices, which were created based on observations from ground-based observatories, were developed. The *AE*, *AL*, and *AU* auroral electrojet indices were introduced in 1966 by analyzing magnetic field variations at 12 observatories located at auroral latitudes (Davis and Sugiura, 1966). We note that the use of only 12 stations in the auroral zone is not sufficient to determine substorm disturbances at high or low latitudes; disturbances of this type will be weakly manifested in the *AE*, *AL*, and *AU* indices. However, with the advent of the large SuperMAG (https://supermag.jhuapl.edu/) network of magnetic

observatories located around the world, this shortcoming was overcome. The *SME* (*SML*, *SMU*) indices calculated from SuperMAG data are similar to the *AE* (*AL*, *AU*) index (Gjerloev, 2009; Newell and Gjerloev, 2011). There is also the IMAGE magnetometer network (https://space.fmi.fi/image/www/), which was established in 1991 to study magnetic disturbances in Scandinavia. The meridional profile of the IMAGE magnetometers extends from subauroral to high latitudes (from ~52 to ~79° latitude). Unlike other indices, geomagnetic indices calculated from IMAGE data are abbreviated as *IE*, *IU*, and *IL* (Viljanen et al., 2006).

Recently, the *MPB* index was proposed (Chu et al., 2015; McPherron and Chu, 2016, 2018). There are two slightly different lists of the *MPB* index since ~1982 that can be found in the supplementary information for the online version of the paper (McPherron and Chu, 2018). Differences in calculation methods are described, for example, in (McPherron and Chu, 2016). The main difference is that the McPherron list is based on data from 35 stations with geomagnetic latitude λ_{mag} between −45° and 45° while the Chu list is based on data from 41 stations in the northern and southern hemispheres with $20° < |\lambda_{mag}| < 52°$. The main advantage of the new index is the use of observations from mid-latitude stations, which makes it possible to track substorm disturbances even in the absence of data at higher latitudes.

We note that various geomagnetic indices, which characterize general planetary disturbances (*Kp*, *Ap*, *ap*, *Am*, *am*, *Aa*, *aa*, *Dst*) (Yanovsky, 1978), are also used to describe the intensity of magnetic storms.

The existence of semi-annual and annual variations in geomagnetic activity was known since the middle of the 19th century (Broun, 1848; Sabine, 1852). Variations are observed at all latitudes. At low latitudes, variations in the *Dst* index are described, for example, in (Cliver et al., 2000; O'Brien and McPherron, 2002). At mid-latitudes, variations in the *Am*, *Ap*, and *Kp* indices were studied in (Berthelier, 1976; Rangarajan and Iyemori, 1997; Nusinov et al., 2015). At auroral latitudes, variations in auroral indices were analyzed in (Sing et al. 2013), where it was shown that *AE*, *AL*, *SME*, and *SML* have a significant seasonal dependence with a maximum on the days of equinoxes while the *AU* and *SMU* indices have only a summer maximum. The frequency of occurrence of substorms were studied in (Fu et al., 2021), and it was shown that the number of substorms is maximal during the equinoxes. Semi-annual variations are more significant for intense substorms. Local indices *IE*, *IL*, and *IU* have similar seasonal characteristics. Seasonal variations in the current strength of the westward and eastward electrojet were studied in (Guo et al. 2014). It was shown that seasonal variations are combinations of annual and semi-annual cycles. Variations in geomagnetic activity at various latitudes, including the polar cap, were compared in (Lyatsky and Tan, 2003). The authors concluded that the absolute amplitude of variations in the *Dst*, *Ap*, *Am*, and *AL* indices is close in magnitude, while the relative amplitude sharply decreases with increasing latitude.

To explain the semi-annual and annual variations in geomagnetic activity, several "geometric" hypotheses based on the mutual orientation of the axes of rotation of the Earth and the Sun, the direction of their magnetic fields, the inclination of the ecliptic, and so on were proposed. These include the Russell–McPherron effect (Russell and McPherron, 1973), the equinoctial effect (McIntosh, 1959; Boller and Stolov, 1970; Svalgaard et al., 2002), the axial effect (Cortie, 1912; Bartels, 1932), and asymmetry effects in the solar wind and solar magnetic hemispheres (Mursula et al., 2011). A detailed discussion of the hypotheses can be found, for example, in (Yoshida, 2009; Lockwood et al., 2020) and references therein. There is still no consensus on which effect makes the main contribution to the observed semi-annual and annual variations in geomagnetic activity. Usually, preference is given to the Russell–McPherron effect, which explains the variations by the relative orientation of the axes of rotation of the Sun and the Earth to the ecliptic plane and by the orientation of the axis of the Earth's magnetic dipole.

In recent decades, statistical methods for analyzing the distribution of geomagnetic indices have been actively developed. In particular, they make it possible to correctly determine the most probable index values. For example, in analyzing the distribution of the *Ap* index it was shown in (Mikhailov et al., 2005) that the distribution reaches a maximum at $Ap \sim 5$, after which an almost exponential decline begins. As well, the probability of extreme events can be estimated. Using a lognormal distribution for the *Dst* index, it was concluded in (Love et al., 2015) that a geomagnetic storm with $Dst \leq -850$ nT (Carrington event, minimal intensity estimate) must occur approximately 1.13 times per century. Assuming a power-law distribution in the region of large negative *Dst* and using an upper estimate of the intensity of the Carrington event ($Dst = -1760$ nT), it was found in (Yermolaev et al. 2013) that such an event can occur no more than once every 500 years. Using the Weibull distribution, extreme events on the Sun and their influence on processes on the Earth were studied in (Gopalswamy, 2018). Estimates were obtained for the parameters of events that can be expected once a century and once a millennium. The distribution of peak *Dst* values during geomagnetic storms was approximated by an exponential law (Echer et al. 2011) and the Pareto distribution (Tsubouchi and Omura, 2007; Riley, 2012). The generalized Pareto distribution was used to study the *AL*, *AU*, and *AE* indices (Nakamura et al., 2015), as well as to analyze variations in the magnetic field in Europe and the rate of its change (Thomson et al., 2011).

In this study, we analyzed the appearance of substorm disturbances for the period from 2007 to 2020 using the methods of statistical processing of magnetic field variations according to the data of the Bulgarian Panagyurishte station (PAG) at middle latitudes and the *IL* index of the auroral electrojet using the IMAGE network at auroral and high geomagnetic latitudes. It should be noted that besides the selection of substorms by visual control of magnetograms, there are software algorithms for their detection, including those based on the analysis of variations in geomagnetic indices. For example, by analyzing variations in the *IL* index, an algorithm was created for detecting substorms using the IMAGE network, in which a substorm is defined as an event when the rapid decrease in *IL* exceeds 80 nT/15 min (Tanskanen et al., 2009). In our study, we used a different criterion, which is described in detail in Section 3. Two samples of substorm events ($IL < -200$ nT) when a positive bay (MPB) was observed or absent in the horizontal component at the PAG station were studied. As well, the obtained results were compared with the results obtained from a sample of isolated substorms at the IMAGE meridian that is based on the list of substorms (Ohtani and Gierloev, 2020).

2. THE DATA

Geomagnetic activity at the Scandinavian IMAGE meridian was determined from the *IL* index, which is calculated by the same method as the *AL* index (Davis and Sugiura, 1966), but from observations of selected stations of the IMAGE network (https://space.fmi.fi/image/www/il_index_panel.php). Here, when calculating the *IL* index, we used two meridional chains of stations PPN-SOR and PPN-NAL. Figure 1 shows a map of IMAGE stations in geographical coordinates, where circles mark IMAGE stations and asterisks indicate stations of the PPN-NAL meridional chain. We note that the PPN-SOR chain consists of 12 stations located from 51.4 (47.1) to 70.5° (67.3°) of geographic (geomagnetic) latitude while the PPN-NAL chain ends to the north, on the Svalbard archipelago, at the NAL station (~78.9° (76.2°) geographical (geomagnetic) latitude), i.e., the PPN-NAL chain consists of four additional stations at high latitudes (https://space.fmi.fi/image/www/station_selection.html). Variations in the *IL*-index calculated from the data of two chains were analyzed for the period from 2007 to 2020. It should be noted that from 2007 to 2014, the meridional chain of stations began at higher latitudes, at the TAR station (~58.2° (54.5°) of geographic (geomagnetic) latitude). Since January 2015, it was extended to lower latitudes, adding two BRZ stations and SUW stations (~54° (50°) geographical (geomagnetic) latitude), and since January 2018, a PPN station was added. However, here, for uniformity, we will designate this chain as PPN-NAL for the entire study period, from 2007 to 2020.

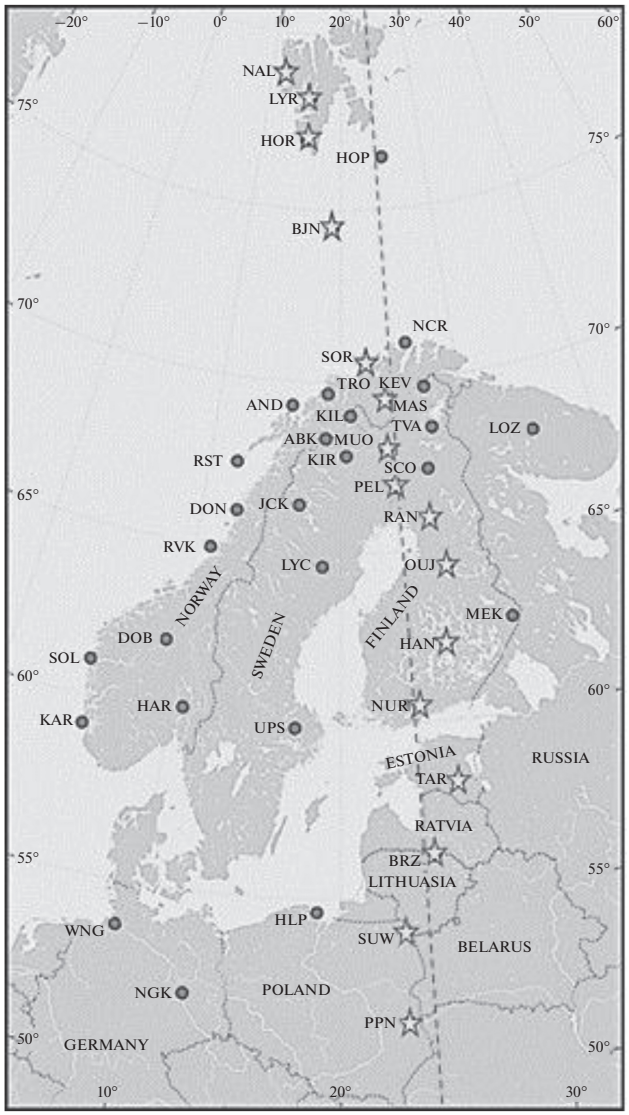

Fig. 1. A map of the locations of IMAGE network magnetometers, circles mark all IMAGE stations, asterisks indicate stations of the PPN-NAL meridional chain. The dotted line marks the meridian, on which the Bulgarian station is located in Panagyurishte.

The mid-latitude positive bays were determined from the data of the Panagyurishte station (~42.5° geographic and ~36.9° geomagnetic latitude), which is located slightly to the west (at the geographic (geomagnetic) longitude ~24.2° (~97.2°)) of the PPN-NAL meridional chain of the IMAGE network, but, in general, it can be considered as a continuation of this chain to lower latitudes. Observation data in Panagyurishte are taken from the INTERMAGNET database (https://intermagnet.github.io). We note that for the period from 2007 to 2020, the data on the magnetic field have only small gaps, except for the time interval from September to October 2017, when a backup magnetometer was installed at the observatory.

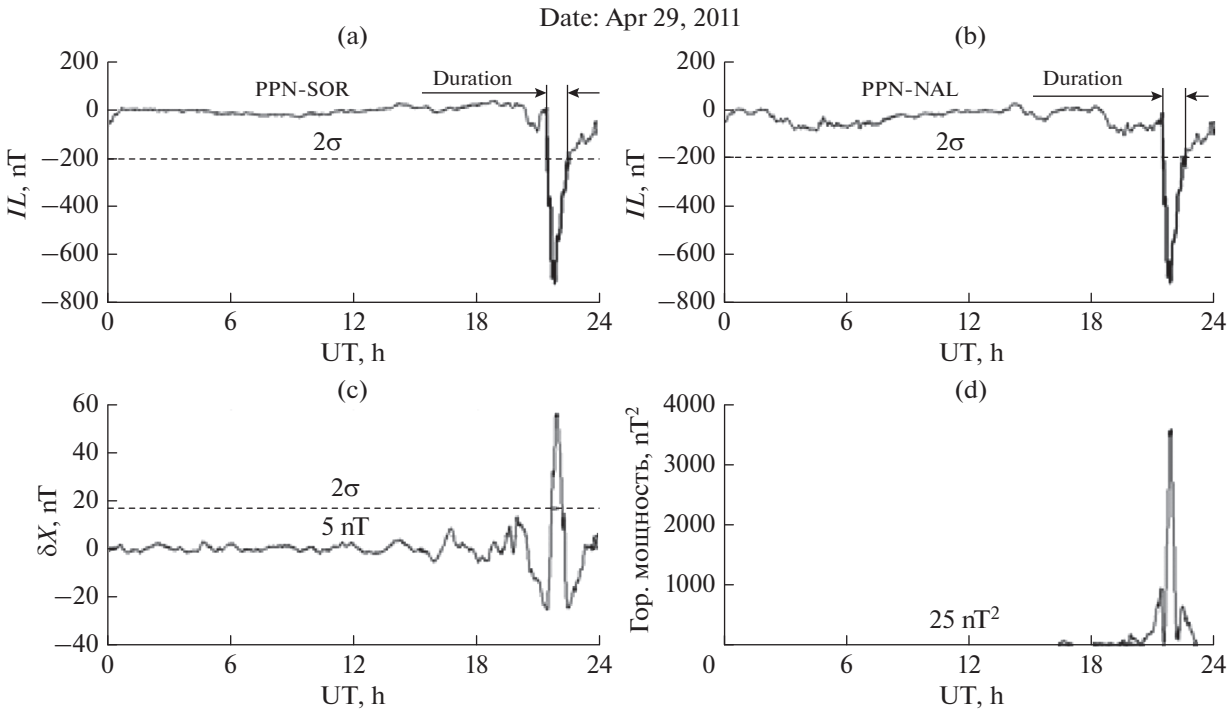

Fig. 2. The event of April 29, 2011: (a) variations of the *IL*-index calculated by the PPN-SOR chain, (b) by the PPN-NAL chain, variations of the *X*-component of (c) the magnetic field and (d) horizontal power at the PAG station. The horizontal dotted lines show the values of 2σ, 5 nT, and 25 nT^2. The "+" signs mark the moments by which the duration of the event was determined.

The data were obtained using a data loading system developed at the National Institute of Geophysics, Geodesy, and Geography, Bulgarian Academy of Sciences (Bojilova, 2017).

Isolated substorms were determined according to the list of events posted on the SuperMAG website (https://supermag.jhuapl.edu/substorms/). The list was created based on the analysis of variations in the *SML* index and contains information on the moment of onset and localization of the strongest substorm disturbances (Ohtani and Gjerloev, 2020). Based on this list from 2010 to 2019, only events that were observed near the meridian of the IMAGE network were selected for the analysis, i.e., from 1800 to 0100 UT (2104 MLT).

3. SELECTION OF EVENTS

In our study, we used the following criterion for determining substorm disturbances: $IL < -200$ nT with a negative peak duration in the *IL* index of at least 10 min. To determine the duration of the event, the variances and standard deviations σ for the *IL* index were calculated for each day. An example of selecting an event for the analysis is given in Fig. 2, which shows the *IL* index for April 29, 2011 that is calculated for the stations of the PPN-SOR chain (Fig. 2a) and for the PPN-NAL chain (Fig. 2b). The horizontal dashed line in the figures shows the lower limit of the 2σ interval, the moments of intersection of the 2σ line with the *IL* graph are shown by "+" crosses, and the interval between them shows the duration of the event. Figure 2c shows the variation of the *X*-component of the magnetic field (denoted as δX in Fig. 2) at the PAG station, and horizontal dotted lines indicate the values of 2σ and 5 nT, which are used to determine the presence of a positive bay at the PAG station. We believe that a positive bay (MPB) was observed only if, near the peak of the *IL* index, the variation of the *X*-component of the magnetic field (δX) exceeded 5 nT and simultaneously exceeded the limit of 2σ, where σ is the square deviation calculated from the variations of the *X*-component for a given day.

It should be noted that stationary magnetospheric convection (SMC) events also fall into our statistics since during these events there may be magnetic disturbances: convective bays (convective substorms). If they are sufficiently intense ($IL < -200$ nT), then they are also included in the statistics since we did not specifically single out or remove them from consideration, i.e., all perturbations exceeding the threshold value of *IL* are considered.

Figure 2d shows the horizontal power of the magnetic field at the PAG station, which actually represents the *MPB* index calculated from the data of a single PAG station only. To calculate the horizontal power, a program was developed based on the algorithm for calculating the *MPB* index (Chu, 2015;

McPherron and Chu, 2017), but with some minor changes. In addition to the initial algorithm, procedures for detecting gaps and peaks in the data were introduced. As well, we replaced the procedure for detecting days with a strong magnetic field used in (McPherron and Chu, 2017) with a procedure based on the Grubbs outlier criterion (Grubbs, 1972). All data processing procedures and calculations are described in detail in (Werner et al., 2021). The dotted horizontal line in Fig. 2d shows the value of 25 nT^2 corresponding to the criterion for selecting a positive bay according to a criterion of $\delta X > 5$ nT since the horizontal power is proportional to the squares of the *X*- and *Y*-components. We note that graphs similar to those shown in Figs. 2c and 2d were plotted for each day and uploaded to the website (https://magnetic.nuclearmodels.net/Catalog_MPB/). Thus, for our statistical studies, two samples of events for substorm disturbances accompanied and not accompanied by positive bays in Panagyurishte were created. The samples were created for the night sector, i.e., from 1800 to 2400 UT (2100 to 0300 MLT), where substorms usually occur. Further in the text, these event samples, where only IMAGE network data are used, will be denoted as IMAGE-PPN-NAL and IMAGE-PPN-SOR.

To compare the results and control that the selected events are substorm disturbances, we took another sample of events. It is based on the list of isolated substorms found on the SuperMAG website (Ohtani and Gjerloev, 2020). This list was created based on variations of the *SML* index and contains information on the onset of isolated substorms from 1995 to 2019. We selected for the analysis only events from 2010 to 2019 when the stations of the IMAGE network were in the night sector. Each moment of the onset of an isolated substorm was associated with the minimal value of the *IL* index observed 2 h after the onset. The *IL*-index was calculated using IMAGE data for two meridional chains of stations PPN-NAL and PPN-SOR. Further, in order to distinguish our event samples, we will designate events according to the list of isolated substorms (IS) as IS-PPN-NAL and IS-PPN-SOR.

4. RESULTS

4.1. Statistical Studies of the Distribution of the IL Index

An important characteristic of a statistical ensemble is its distribution. Figure 3a shows the histograms of the *IL* index obtained from the IMAGE-PPN-NAL (black) and IMAGE-PPN-SOR (gray) event samples. For the entire studied interval (2007–2020), the *IL* index values were sorted by intensity and distributed by class. The class width was chosen to be 50 nT. We note that the PPN-NAL event sample includes the PPN-SOR sample, but is about a third larger.

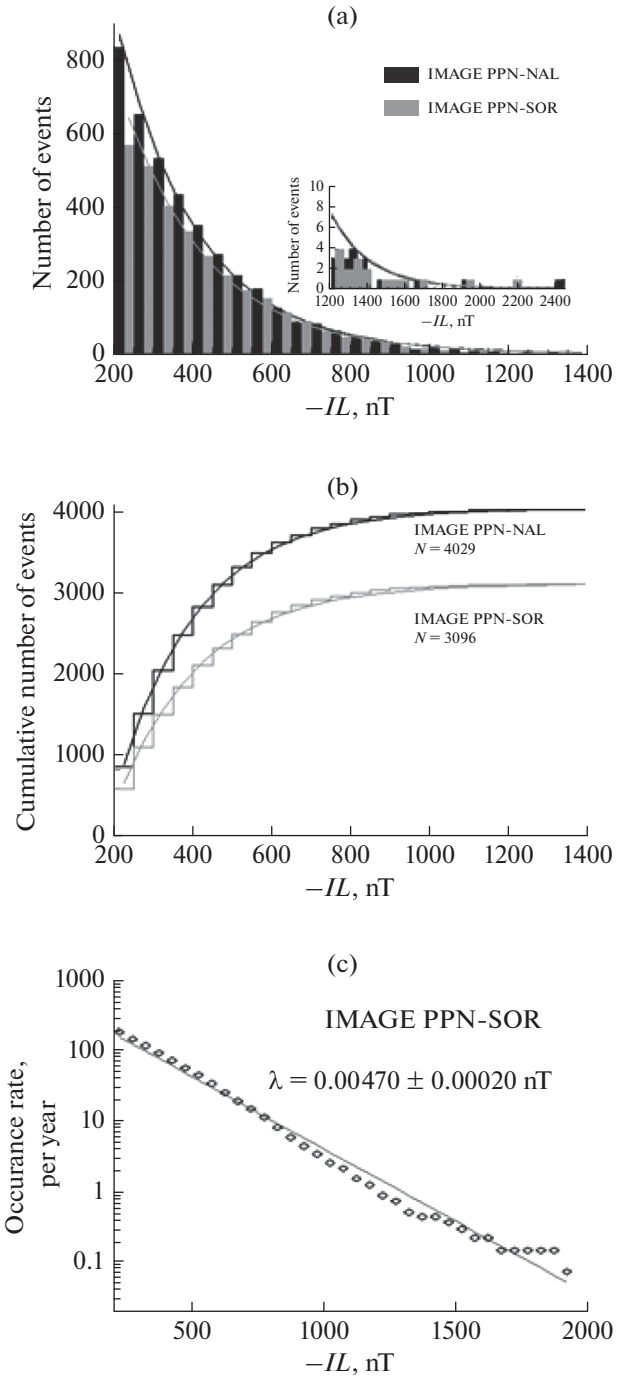

Fig. 3. Histograms of the *IL* index calculated from two chains PPN-SOR (grey) and PPN-NAL (black). Solid lines show their approximations by exponential distributions. (a) Histograms of large values of $IL < -1200$ nT are presented in the insert. (b) Empirical cumulative frequency and theoretical cumulative frequency calculated with same parameter λ. Rate of events per year for PPN-NAL. The empirical dependence is shown by circles, and the theoretical approximation is shown by a solid line (c).

It can be seen that both histograms IMAGE-PPN-NAL and IMAGE-PPN-SOR decrease almost exponentially. An insert of Figure 3a shows events with $IL < -1200$ nT in more detail. It can be seen that there were only a few intense events. In this case, events with $IL < -2200$ nT belong to the supersubstorm on September 7–8, 2017. This is one of several supersubstorms that were observed when the IMAGE stations were in the night sector, and extremely strong magnetic field disturbances were recorded (Despirak et al., 2020).

Both IMAGE-PPN-NAL and IMAGE-PPN-SOR histograms were fitted with an exponential distribution. An empirical f probability density function (DPF) is obtained from the normalized N_i/A histogram.

Theoretical exponential DPF is given by the expression:

$$f_{\exp}(x) = \lambda \exp^{-\lambda x} \quad x \geqq 0, \tag{1}$$

where x in our case is equal to $x = -(IL + 200$ nT) and $IL \leq -200$ nT. The midpoints of the intervals should be taken as x values.

The empirical F_i cumulative distribution function (CDF) is given by simple summation: $F_i = \sum_{j=1}^{i} N_j / N$. Theoretical CDF F is given by the formula: $F(x) = \int_{-\infty}^{x} f(t)\,dt$. For exponential CDF, we obtain that

$$F_{\exp}(x) = 1 - \exp^{-\lambda x} \quad x \geq 0 \tag{2}$$

and it determines probability $P(X < x)$ of random variable X. The λ parameter can be estimated as $\frac{1}{\overline{x}}$ to make empirical CDF match the theoretical one.

Empirical CDFs for both chains are shown in Figs. 3b together with their approximation by theoretical exponential function CDF. It can be seen that both distributions are very similar while the parameters $\lambda_{\text{PPN-SOR}} = 0.00465$/nT and $\lambda_{\text{PPN-NAL}} = 0.00487$/nT are almost identical. Using the Kolmogorov-Smirnov test for two samples, we confirmed that the distributions do not differ at a significance level of 0.05. This means that they come from the same statistical ensemble.

The $P(X > x)$ probability that random variable X is greater than certain x is defined as $1 - P(X > x) = 1 - F(x)$, and for the exponential distribution, we obtain that $P(X > x) = \exp^{-\lambda x}$. Thus, the graphical representation of $\sum_{j=1}^{i} N_j / N$ on a logarithmic scale for an exponential distribution is a straight line with slope λ.

Figure 3c shows the intensity of the flow of events, i.e., the number of observations with an IL index less than a certain IL value that is referred to 1 year. The slope of the straight line in this graphical representation is λ/y, where y is the number of years of observation. Figure 3c shows that the frequency of occurrence of events with $IL \sim -1500$ nT is four events per 10 years, for events with $IL < -1750$, it is once every 10 years. We note that this was obtained only for the selected meridional chain and the MLT-limited sector (from 21–24 h).

We consider the distribution of substorm events when positive bays (MPBs) were recorded at Panagyurishte station and when no MBP bays were observed. The distribution histograms of the IL-index for events with positive bays (gray) and without them (black) are shown in Figs. 4. The number of cases without MBPs decreases monotonically as the IL modulus increases. The IL distribution for cases with MPBs initially increases with increasing IL modulus so that, at ~–300 nT, there is an almost equal number of events with and without MBPs. At $IL < -600$ nT, almost all events are accompanied by mid-latitude MPB bays. Figure 4b shows similar histograms for the cumulative number of events, and the format of Fig. 4b is similar to the format of Fig. 4a. As can be seen, the cumulative CDF for events without positive MPB bays saturates very quickly and does not exceed ~35% of all events. Accordingly, events accompanied by mid-latitude positive bays were observed in ~65% of cases.

The Weibull distribution (Weibull, 1951; Coles, 2001) is well suited to describe the empirical course of the IL index. We note that although the distributions of the IL index without MPB bays can be also described by an exponential, it turned out that the use of the Weibull distribution produces a much better approximation. Various parameterizations are known for the Weibull distribution. We use the following PDF definition:

$$f_{\text{Weib}}(x) = \alpha\beta[(\alpha x)^{\beta-1}]\exp[-(\alpha x)^{\beta}]. \tag{3}$$

The CDF cumulative function has the form:

$$F_{\text{Weib}}(x) = 1 - \exp[-(\alpha x)^{\beta}]. \tag{4}$$

The α and β distribution parameters were obtained using the Statistica program. For events where there were no positive MPB bays, we found that $\alpha = 0.00996$ and $\beta = 1.0334$, and for events with accompanying MPB bays, we found that $\alpha = 0.00340$ and $\beta = 1.3154$. The empirical CDF is shown in Fig. 4b together with the theoretical one calculated by equation (4). As can be seen from the graph, the Weibull distributions are suitable for describing the observed distribution of the IL index. This is not surprising since defining $IL(t)$ as the minimum value of $IL_n(t)$, where n is the station number, leads to an extreme distribution of IL values. One of the three main types of extreme value distributions is the Weibull distribution. It should be noted that the exponential distribution is a special case of the Weibull distribution at $\beta = 1$. Indeed, the value of $\beta = 1.0334$ observed for the distribution for events when there were no accompanying MPBs looks like an

exponential distribution and β does not deviate significantly from unity. Thus, all distributions of the *IL* index of the auroral electrojet (*IL* < −200 nT), both for the sample of events for the entire period of 2007–2020 and for samples with and without positive MPB bays, can be described by the Weibull distributions of extreme values.

4.2. Annual and Semi-Annual Variations

We consider semi-annual and annual variations of the IL-index for our event samples. Figure 5 shows the monthly distribution of the *IL* index obtained for isolated substorms in the period from 2010 to 2019. The *IL* index was calculated in two ways: from the data of all Scandinavian stations (excluding Svalbard) (gray) or from the data of the PPN-NAL chain (black color). As can be seen, a seasonal dependence is observed for any method of calculating the *IL* index. As well, autumn-spring maxima were observed both for all events (Fig. 5a) and for events divided into various classes by intensity *IL*: 200 nT ≤ *IL* < −400 nT, −400 nT ≤ *IL* < −600 nT, −600 nT ≤ *IL* < −800 nT, −800 nT ≤ *IL* < −1000 nT, and *IL* ≤ −1000 nT (Figs. 5b–5f). In this case, the amplitude of seasonal variations was ~40 cases, which corresponds to ~25% of the average monthly value. During the maxima of the equinoxes, ~200 substorms were observed, and during the summer minimum, ~120 substorms were observed. As can be seen in Figs. 5b–5f, at an increase in the intensity of the westward auroral electrojet, the semiannual effect becomes more pronounced: the summer minimum disappears, and autumn–spring maxima predominate.

It is interesting to compare the seasonal course for the events of isolated substorms and for the events with accompanying positive bays at Panagyurishte station. The monthly distribution of the normalized number of events for cases with MPBs is shown in Fig. 6 (the format of Fig. 6 is similar to that of Fig. 5). The *IL* index was calculated from the data of two chains of stations: PPN-SOR (grey) and PPN-NAL (black). For both distributions, the seasonal dependence is clearly visible: the presence of an autumn and spring maximum, but the amplitude of seasonal fluctuations is slightly larger for events calculated using the PPN-SOR chain than that using PPN-NAL. As well, the maxima of the equinoxes are between 0.11 and 0.12, with the summer minimum being ~0.045. The maximum deviations from the mean annual value is 0.0833, the difference of 0.115–0.08 is ~45%, which is almost two times greater than that obtained for the distribution of events of isolated substorms (Fig. 5).

From the monthly distribution, annual and semi-annual variations were identified using the Fourier harmonics, the result is shown in Fig. 7 for two samples of events when the *IL* index was calculated using the PPN-NAL (Fig. 7a) and PPN-SOR (Fig. 7b) chain. Seasonal variations are shown by a solid thick line and the annual and semi-annual variations separated from them are shown by dotted and dash-dotted lines, respectively. The sum of the annual and semi-annual components is shown by a thin solid line. Annual and semi-annual variations were extracted using Fourier harmonics from the monthly distribution (Fig. 6) as follows:

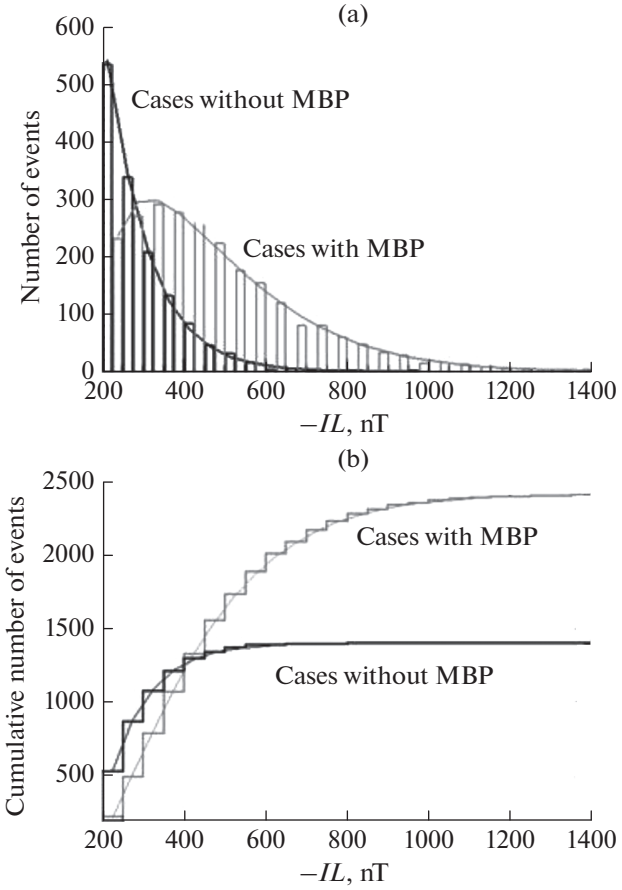

Fig. 4. *IL* index distribution histograms for events with a positive bay (MPB) in Panagyurishte (grey) and without a positive bay (black). The solid lines show the approximation of (a) histograms by the Weibull distribution; (b) similar histograms for the cumulative number of events.

$$RN(n) = a_{an}\sin\left(\frac{2\pi n}{T}\right) + b_{an}\cos\left(\frac{2\pi n}{T}\right) + a_{san}\sin\left(\frac{2\pi n}{\frac{T}{2}}\right) + b_{san}\cos\left(\frac{2\pi n}{\frac{T}{2}}\right) + \varepsilon(n) \quad (5)$$

@для $n = 0,\ldots,11.$

The coefficients of determination (R^2) are 0.952 and 0.975 for the PPN-NAL and PPN-SOR chains, respectively. Using Student's criterion, we checked the significance of the coefficients of the harmonic Fourier series. It turned out that for both groups of events (Figs. 7a and 7b), only the term with cosine (cos) is

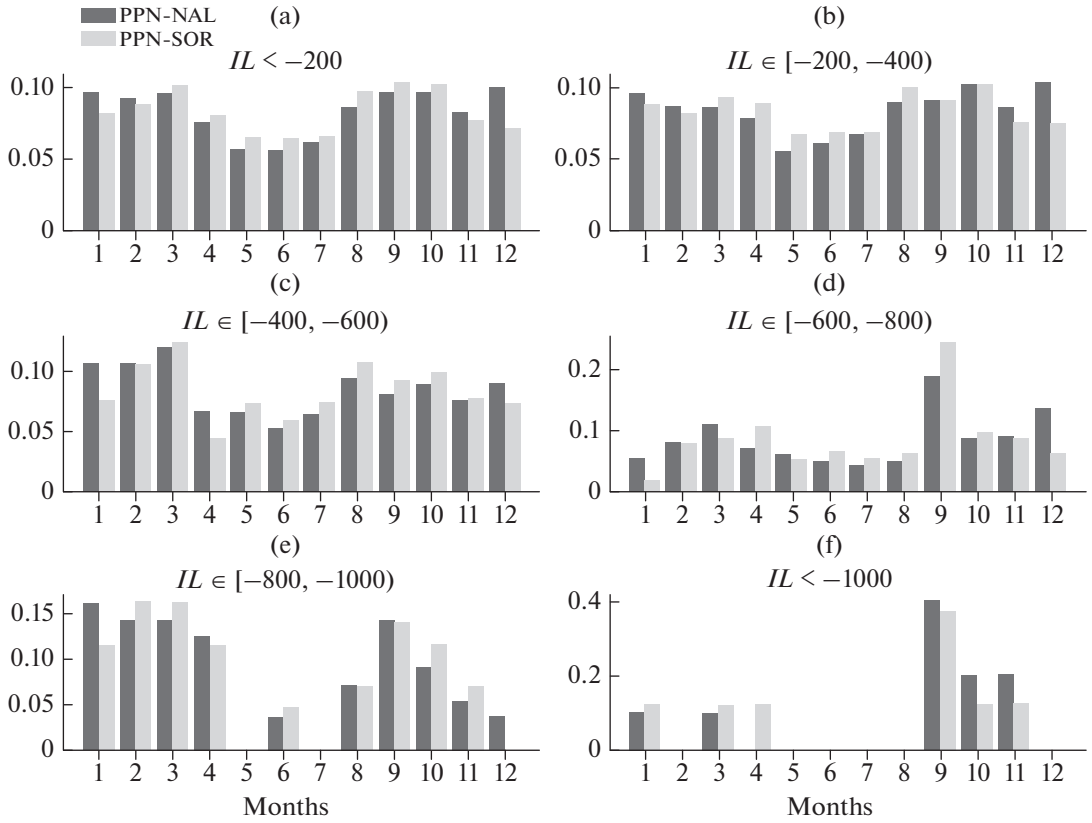

Fig. 5. The monthly distribution of the *IL* index for events in the list of isolated substorms during 2010–2019. The *IL* index was calculated for all Scandinavian stations (excluding Svalbard) (gray bars) and for the chain of PPN-NAL stations (black bars): (a) for all events with $IL < -200$ nT; (b, c, d, e, f) for events divided into classes: -200 nT $\le IL < -400$ nT, -400 nT $\le IL < -600$ nT, -600 nT $\le IL < -800$ nT, -800 nT $\le IL < -1000$ nT, and $IL \le -1000$ nT.

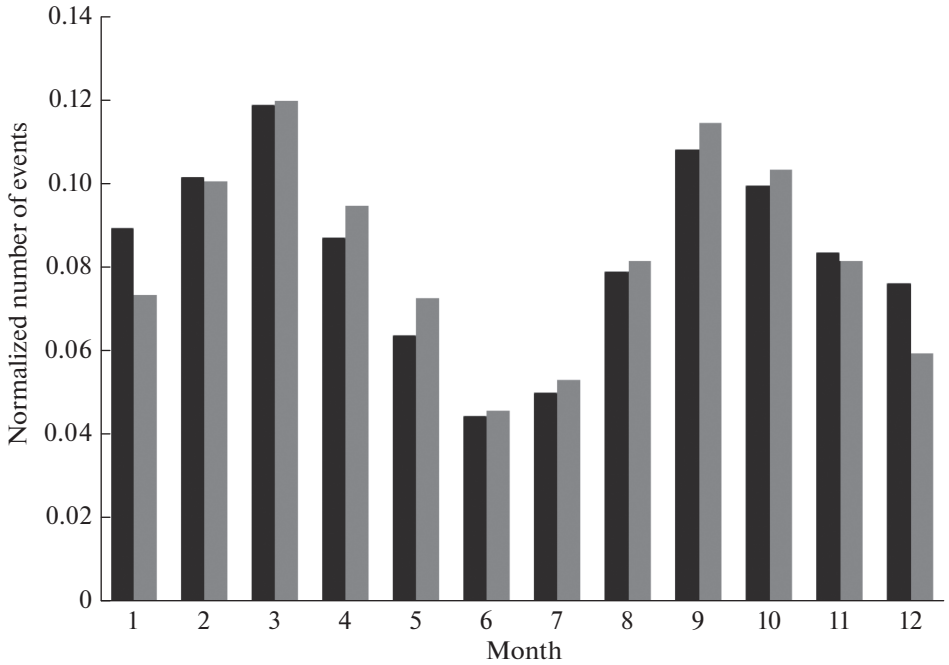

Fig. 6. The format of the drawing is similar to the format of Fig. 5. The monthly distribution of the normalized number of IL-index cases during positive bay events (MPBs) in Panagyurishte. The *IL* index along the PPN-SOR chain is shown by gray bars, along the PPN-NAL chain is shown by black bars.

significant in the annual variation, and the significance level is 0.05. The residual values of $\varepsilon(n)$ do not show any periodic changes and are randomly distributed.

Figure 7 shows that the sum of annual and semi-annual variations (thin line) is in good agreement with the initial monthly distribution (thick line). The coefficients of determination are 0.952 and 0.975 for the PPN-NAL and PPN-SOR chain, respectively. As can be seen, the annual variation has a summer minimum and a winter maximum, and the variations are stronger for the PPN-NAL chain, which is possibly associated with greater illumination in the summer months in the north. Semi-annual variations show maxima at the time of the equinoxes. The semi-annual variation of the equinox maximum for the PPN-SOR chain is ~0.30 and is slightly stronger than the variations observed for the PPN-NAL chain, where the equinox maximum is ~0.25. A more detailed calculation shows that the maxima do not fall exactly on the equinoxes, but are observed on April 3/October 3 for the PPN-NAL chain and on April 7/October 6 for the PPN-SOR chain.

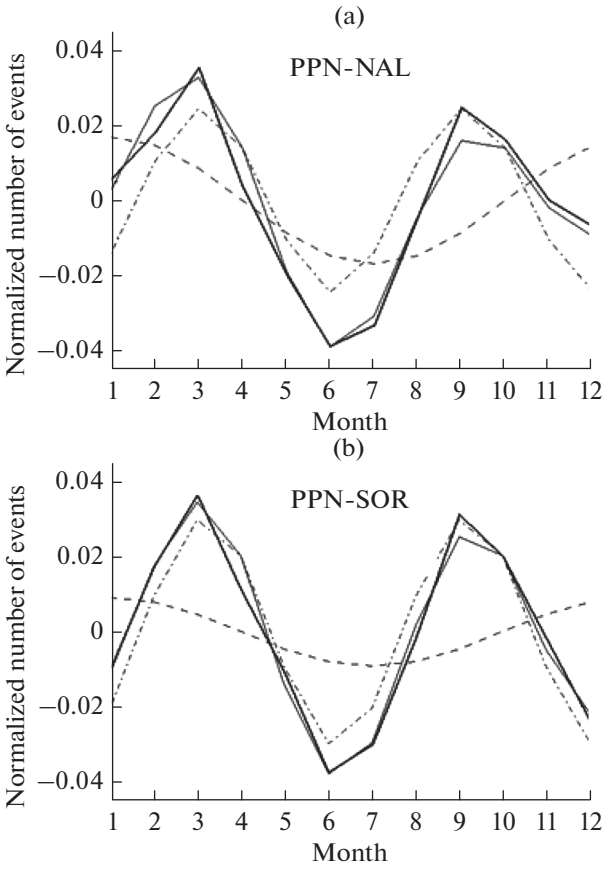

Fig. 7. The monthly distribution of the normalized number of *IL*-index cases (thick black line) for different chains: (a) PPN-SOR; (b) PPN-NAL; annual (dashed) line and semi-annual (dashed-dotted) line. The line of approximation of the sums of the annual and semi-annual components (thin line): (a) for the monthly values of the PPN-SOR chain and (b) for the monthly values of the PPN-NAL chain.

5. DISCUSSION

For the 2007–2020 period, the distributions of the *IL* index and the cumulative distribution function for a sample of events with $IL < -200$ nT (IMAGE-PPN-NAL and IMAGE-PPN-SOR) were obtained, and the occurrence of extreme events was estimated (Fig. 3). It can be seen that the distribution of the *IL* index contains only a few events of intense substorms with $IL < -1500$ nT. This is explained by the fact that a rather narrow longitudinal interval of event registration was chosen (the PPN-NAL and PPN-SOR meridional chains) and a limited MLT sector (from 2100 to 0300). It turned out that over 14 years, only five events with $IL < -1500$ nT were recorded on the PPN-SOR chain in the interval of 1800–2400 UT, i.e., 0.35 events per year. This value is somewhat underestimated, since it is known that there are substorms with $IL < -2000$–2500 nT. However, the aim of this study was not to show the general distribution of events by intensity, but to study the relation between substorms observed in the auroral zone, at the IMAGE meridian, and positive bays at middle latitudes, at Panagyurishte station.

After analyzing events with and without MPBs for 2007–2020, we found that there were ~two times fewer events without positive MPB bays than events with MPBs (Fig. 4). The cumulative function (CDF) for events without positive MPB bays was ~35%, i.e., ~65% of the events were accompanied by mid-latitude positive bays. It is known that positive bays at middle latitudes are an indicator of the presence of a substorm current wedge (McPherron et al., 1973; Kepko et al., 2015), and, therefore, it can be argued that the selected events were substorms in 65% of cases. Figure 3 shows that, at an increase in the event intensity, the fraction of the cumulative function without positive MPB bays sharply decreases, and starting from $\sim IL < -600$ nT, almost all events were accompanied by positive bays, i.e., were substorm disturbances.

In our opinion, it is interesting to compare the obtained results with the results obtained from cases that were known to be substorms, i.e., based on a sample of isolated substorms (Ohtani and Gjerloev, 2020), which were observed at the same IMAGE meridian in the period 2009–2019, in the night sector (from 1800 to 0100 UT). The result of the statistical study is shown in Fig. 8, where histograms of the *IL* index are shown; the format of Fig. 8 is similar to the format of Fig. 3, IS-PPN-SOR calculations are shown in gray, and IS-PPN-NAL calculations are shown in black. These distributions are also suitable to be described by the Weibull distribution while the distribution of events for the IS-PPN-NAL chain is closer to the exponential distribution and for the IS-PPN-SOR chain is closer

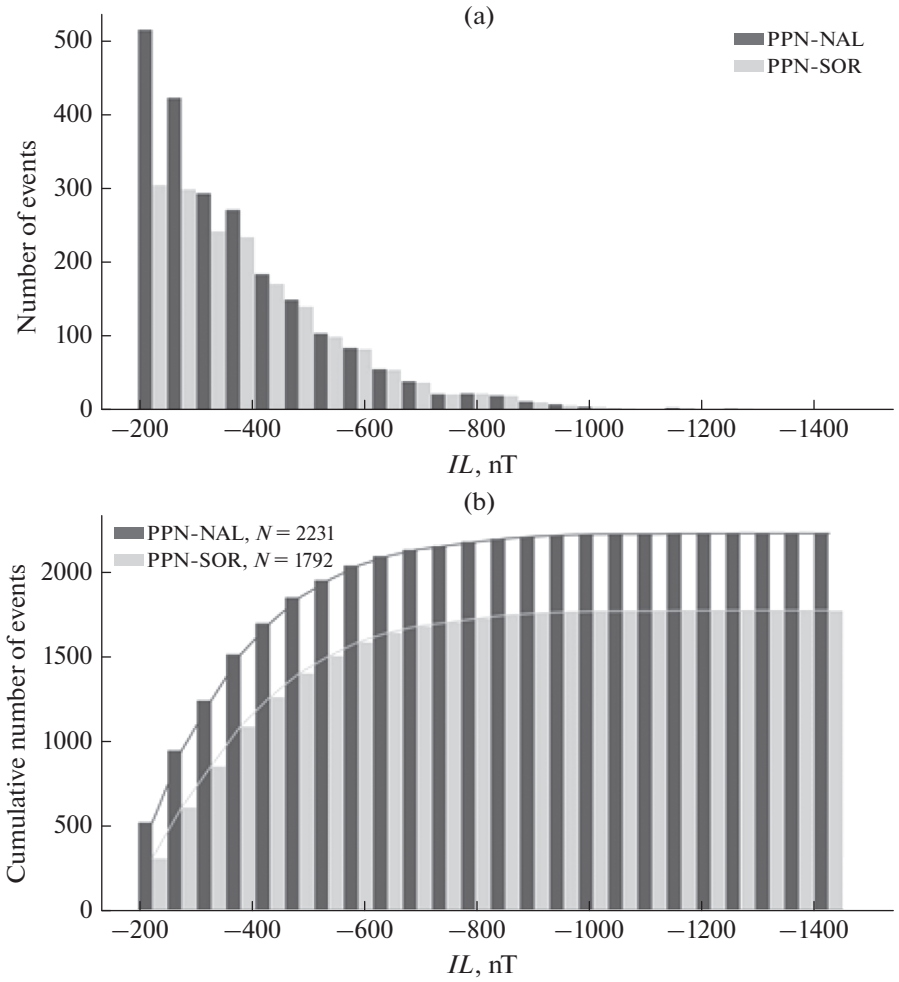

Fig. 8. Histograms of (a) the *IL* index and (b) the cumulative number of events for isolated substorms, the format of the figure is similar to that of Figs. 3a and 3b. The *IL* index was calculated using two chains IS-PPN-SOR (grey) and IS-PPN-NAL (black).

to the distribution of events with accompanying positive bays (MPBs). The difference in the results for the two chains of stations may be due to the fact that the IS-PPN-NAL distribution is affected by substorms that are observed at very high latitudes over Svalbard, the so-called polar substorms (Despirak et al., 2014). Although it was shown that these substorms are also accompanied by positive bays, but these bays were often observed at latitudes higher the Panagyurishte station (Despirak et al. 2022).

Figure 8b shows the cumulative event distribution functions for two different chains of stations, PPN-NAL and PPN-SOR. We note that the number of isolated substorms was approximately two times less than the number of events shown in Fig. 3. It should be noted that the list of isolated substorms (Ohtani and Gjerloev, 2020) does not include all substorm events since one of the conditions is the onset of a substorm against a relatively quiet background ($SML > -100$ nT for -30 min $\le T \le -1$ min). This condition actually limits the number of intense substorms since they normally begin against the background of disturbed conditions ($SML < -100$ nT).

For our two samples of events: isolated substorms (IS-PPN-NAL and IS-PPN-SOR) and events with positive bays (IMAGE-PPN-SOR and IMAGE-PPN-NAL), seasonal variations were analyzed, from which the annual and semi-annual variations were selected (Figs. 5–7). The annual variations for the PPN-NAL chain are stronger than those for the PPN-SOR chain due to the higher illumination during the summer months in the north. It was shown that the IL index also has a seasonal variation with maxima near the equinoxes, similar to other geomagnetic indices (Sing et al., 2013). As well, this effect becomes more pronounced as *IL* increases, which is consistent with the results of (Fu et al., 2021), where semi-annual variations were shown to be more significant for intense substorms. A comparison of the results obtained for two different samples of events (Figs. 5 and 6) leads to the conclusion that a stronger semi-annual variation is observed for events with accompanying positive bays

than for events of isolated substorms. In this case, the appearance of maxima of semi-annual variations in April and October may be associated with the Russell-McPherron effect.

The *IL* index used in this study primarily characterizes the level of geomagnetic activity. We note that the rate of change in geomagnetic activity is also of great importance. An estimate of statistical distributions of geomagnetic field variability is important, for example, for estimating the probabilities of dangerous levels of GIC in power lines (Vorobiev et al. 2019; Despirak et al. 2022). This is an important issue that should be explored in more detail in future work.

6. CONCLUSIONS

A statistical analysis of geomagnetic activity for two samples of events at the IMAGE meridian showed that:

(1) The empirical distributions for the IMAGE-PPN-NAL and IMAGE-PPN-SOR events are described well by exponential functions, while the distributions for the PPN-NAL and PPN-SOR chains are statistically indistinguishable. The intensity of the flow of events was determined: the frequency of occurrence of events with $IL < -1500$ nT is ~0.35 events/year.

(2) The empirical distributions for events with accompanying positive MPB bays at st. Panagyurishte (IMAGE-PPN-SOR) and empirical distributions for isolated substorms (IS-PPN-NAL and IS-PPN-SOR) are described by the Weibull distribution, which indicates that these are events from the same statistical ensembles.

(3) In ~65% of IMAGE-PPN-NAL cases, events were observed accompanied by mid-latitude positive bays, i.e., these were substorm disturbances.

(4) The annual and semi-annual variations are distinguished for both samples of events. The semi-annual variation has maxima near the equinox days, which, in our opinion, is associated with the Russell-McPherron effect. In this case, for the IMAGE-PPN-SOR sample with MPBs, the variations are stronger than those for isolated substorms.

(5) The annual variations have a summer minimum and a winter maximum, and for events along the PPN-NAL chain, the variations are stronger than those for the PPN-SOR chain due possibly to greater illumination in the summer months at high latitudes.

7. ACKNOWLEDGMENTS

The authors are grateful to the creators of the database IMAGE (http://space.fmi.fi/image/), SuperMAG (http://supermag.jhuapl.edu/), INTERMAGNET (https://intermagnet.github.io/) for possibility of their use in the study. We are also grateful for the opportunity to use the list of isolated substorms obtained by the Ohtani and Gjerloev method (Ohtani and Gjerloev, 2020), the *SMU* and *SML* indices (Newell and Gjerloev, 2011) and collaboration with SuperMAG (Gjerloev et al. 2012). We express our gratitude to the Institute of Geophysics, Geodesy and Geography, Bulgarian Academy of Sciences and the team of employees who provide support for the operation of the instruments at the Panagyurishte observatory (Bulgaria) and for the opportunity to use data from the Panagyurishte observatory.

FUNDING

The work of Verner R., Gineva V., Atanasov A., Bozhilova R., Raikova L., and Valev D. was supported the National Science Foundation of Bulgaria, project no. KP-06-Rusiya/15. The work of Despirak I.V., Lyubchich A.A., and Setsko P.V. was supported by the Russian Foundation for Basic Research and the National Science Foundation of Bulgaria, project no. 20-55-18003.

CONFLICT OF INTEREST

The authors declare that they have no conflicts of interest.

REFERENCES

Akasofu, S.-I. and Meng, C.I., A study of polar magnetic substorms, *J. Geophys. Res.*, 1969, vol. 74, no. 1, pp. 293–313. https://doi.org/10.1029/JA074i001p00293

Bartels, J., Terrestrial-magnetic activity and its relation to solar phenomena, *Terr. Magn. Atmos. Electr.*, 1932, vol. 37, no. 1, pp. 1–52. https://doi.org/10.1029/TE037i001p00001

Berthelier, A., Influence of the polarity of the interplanetary magnetic field on the annual and the diurnal variations of magnetic activity, *J. Geophys. Res.: Space Phys.*, 1976, vol. 81, no. 25, pp. 4546–4552. https://doi.org/10.1029/JA081i025p04546

Boller, B.R. and Stolov, H.L., Kelvin Helmholtz instability and the semiannual variation of geomagnetic activity, *J. Geophys. Res.*, 1970, vol. 75, no. 31, pp. 6073–6084. https://doi.org/10.1029/JA075i031p06073

Bozhilova, R., Automated Geophysical Data Collection System: Appendix XLV, in *Sbornik na "Natsionalna konferentsiya po v"prosi na obuchenie po fizika"* (Proceedings of the National Conference on Issues of Physics Learning), Sofia, 2017, pp. 55–59.

Broun, J.A., Observations in magnetism and meteorology made at Makerstoun in Scotland, in 1844. The Aurora Borealis, *Trans. R. Soc. Edinburgh*, 1848, vol. 18, pp. 401–402. https://doi.org/10.1017/S0080456800039077

Chu, X., Configuration and generation of substorm current wedge, *PhD (Geophysics and Space Physics) Dissertation*, Los Angeles: University of California, 2015.

Coles, S., *An Introduction to Statistical Modeling of Extreme Values*, London: Springer, 2001.

Cortie, A.L., Sun-spots and terrestrial magnetic phenomena, 1898–1911: The cause of the annual variation in magnetic disturbances, *Mon. Not. R. Astron. Soc.*, 1912, vol. 73, no. 1, pp. 52–60. https://doi.org/10.1093/mnras/73.1.52

Davis, T.N. and Sugiura, M., Auroral electrojet activity index AE and its universal time variations, *J. Geophys. Res.*, 1966, vol. 71, no. 3, pp. 785–801. https://doi.org/10.1029/JZ071i003p00785

Despirak, I.V., Lyubchich, A.A., and Kleimenova, N.G., Polar and high latitude substorms and solar wind conditions, *Geomagn. Aeron. (Engl. Transl.)*, 2014, vol. 54, no. 5, pp. 575–582. https://doi.org/10.1134/S0016793214050041

Despirak, I.V., Kleimenova, N.G., Gromova, L.I., Gromov, S.V., and Malysheva, L.M., Supersubstorms during storms of September 7–8, 2017, *Geomagn. Aeron. (Engl. Transl.)*, 2020, vol. 60, no. 3, pp. 292–300. https://doi.org/10.1134/S0016793220030044.

Despirak, I.V., Setsko, P.V., Sakharov, Ya.A., Lyubchich, A.A., Selivanov, V.N., and Valev, D., Observations of geomagnetic induced currents in northwestern Russia: Case studies, *Geomagn. Aeron. (Engl. Transl.)*, 2022a, vol. 62, no. 6, pp. 711–723. https://doi.org/10.1134/S0016793222060032

Despirak, I.V., Kleimenova, N.G., Lubchich, A.A., Malysheva, L.M., Gromova, L.I., Roldugin, A.V., and Kozelov, B.V., Magnetic substorms and auroras at the polar latitudes of Spitsbergen: Events of December 17, 2012, *Bull. Russ. Acad. Sci.: Phys.*, 2022b, vol. 86, no. 3, pp. 266–274. https://doi.org/10.3103/S1062873822030091

Echer, E., Gonzalez, W.D., and Tsurutani, B.T., Statistical studies of geomagnetic storms with peak Dst ≤ –50 nT from 1957 to 2008, *J. Atmos. Sol.-Terr. Phys.*, 2011, vol. 73, nos. 11–12, pp. 1454–1459. https://doi.org/10.1016/j.jastp.2011.04.021

Fu, H., Yue, C., Zong, Q.-G., Zhou, X.-Z., and Fu, S., Statistical characteristics of substorms with different intensity, *J. Geophys. Res.: Space Phys.*, 2021, vol. 126, no. 8, e2021JA029318. https://doi.org/10.1029/2021JA029318

Gjerloev, J.W., A global ground-based magnetometer initiative, *Eos Trans. Am. Geophys. Union*, 2009, vol. 90, pp. 230–231. https://doi.org/10.1029/2009EO270002

Gjerloev, J.W., The SuperMAG data processing technique, *J. Geophys. Res.*, 2012, vol. 117, A09213. https://doi.org/10.1029/2012JA017683

Gopalswamy, N., Chapter 2—extreme solar eruptions and their space weather consequences, in *Extreme Events in Geospace (Origins, Predictability, and Consequences)*, Buzulukova, N., Ed., Elsevier, 2018, pp. 37–63. https://doi.org/10.1016/B978-0-12-812700-1.00002-9.

Grubbs, F.E. and Beck, G., Extension of sample sizes and percentage points for significance tests of outlying observations, *Technometrics*, 1972, vol. 14, no. 4, pp. 847–854. https://doi.org/10.2307/1267134

Guo, J., Feng, X., Pulkkinen, T.I., Tanskanen, E.I., Xu, W., Lei, J., and Emery, B.A., Auroral electrojets variations caused by recurrent high-speed solar wind streams during the extreme solar minimum of 2008, *J. Geophys. Res.*, 2012, vol. 117, no. A4, p. A04307. https://doi.org/10.1029/2011JA017458

Guo, J., Liu, H., Feng, X., Pulkkinen, T.I., Tanskanen, E.L., Liu, C., Zhong, D., and Wang, Z., MLT and seasonal dependence of auroral electrojets: IMAGE magnetometer network observations, *J. Geophys. Res.: Space Phys.*, 2014, vol. 119, no. 4, pp. 3179–3188. https://doi.org/10.1002/2014JA019843

Kepko, L., McPherron, R.L., Amm, O., Apatenkov, S., Baumjohann, W., Birn, J., Lester, M., Nakamura, R., Pulkkinen, T.I., and Sergeev, V., Substorm current wedge revisite, *Space Sci. Rev.*, 2015, vol. 190, pp. 1–46. https://doi.org/10.1007/s11214-014-0124-9

Lockwood, M., Owens, M.J., Barnard, L.A., Haines, C., Scott, C.J., McWilliams, K.A., and Coxon, J.C., Semi-annual, annual and universal time variations in the magnetosphere and in geomagnetic activity: 1. Geomagnetic data, *J. Space Weather Space Clim.*, 2020, vol. 10, p. 23. https://doi.org/10.1051/swsc/2020023

Love, J.J., Rigler, E.J., Pulkkinen, A., and Riley, P., On the lognormality of historical magnetic storm intensity statistics: Implications for extreme-event probabilities, *Geophys. Res. Lett.*, 2015, vol. 42, no. 16, pp. 6544–6553. https://doi.org/10.1002/2015GL064842

Matzka, J., Stolle, C., Yamazaki, Y., Bronkalla, O., and Morschhauser, A., The geomagnetic *Kp* index and derived indices of geomagnetic activity, *Space Weather*, 2021, vol. 19, no. 5, e2020SW002641. https://doi.org/10.1029/2020SW002641

McIntosh, D.H., On the annual variation of magnetic disturbances, *Philos. Trans. R. Soc., A*, 1959, vol. 251, no. 1001, pp. 525–552. https://doi.org/10.1098/rsta.1959.0010

McPherron, R.L., Growth phase of magnetospheric substorms, *J. Geophys. Res.*, 1970, vol. 75, no. 28, pp. 5592–5599. https://doi.org/10.1029/JA075i028p05592

McPherron, R.L., The use of ground magnetograms to time the onset of magnetospheric substorms, *J. Geomagn. Geoelectr.*, 1978, vol. 30, no. 3, pp. 149–163. https://doi.org/10.5636/jgg.30.149

McPherron, R.L. and Chu, X., The mid-latitude positive bay and the MPB index of substorm activity, *J. Geophys. Res.*, 2017, vol. 206, pp. 91–122. https://doi.org/10.1007/s11214-016-0316-6

McPherron, L.R. and Chu, X., The midlatitude positive bay index and the statistics of substorm occurrence, *J. Geophys. Res.: Space Phys.*, 2018, vol. 123, no. 4, pp. 2831–2850. https://doi.org/10.1002/2017JA024766

McPherron, R.L., Russell, C.T., and Aubry, M.P., Satellite studies of magnetospheric substorms on August 15, 1968: 9. Phenomenological model for substorms, *J. Geophys. Res.*, 1973, vol. 78, no. 16, pp. 3131–3149. https://doi.org/10.1029/ja078i016p03131.

Mikhailov, A.V., Depuev, V.Kh., and Leschinskaya, T.Yu., Geomagnetic activity threshold for F2-layer negative storms onset: Seasonal dependence, *Int. J. Geomagn. Aeron.*, 2005, vol. 6, no. 1. https://doi.org/10.1029/2005GI000098

Murayama, T., Origin of the semiannual variation of geomagnetic Kp indices, *J. Geophys. Res.: Space Phys.*, 1974, vol. 79, no. 1, pp. 297–300. https://doi.org/10.1029/JA079i001p00297

Mursula, K., Tanskanen, E., and Love, J., Spring–fall asymmetry of substorm strength, geomagnetic activity and solar wind: Implications for semiannual variation and solar hemispheric asymmetry, *Geophys. Res. Lett.*, 2011, vol. 38, no. 6, p. L06104. https://doi.org/10.1029/2011GL046751

Nakamura, M., Yoneda, A., Oda, M., and Tsubouchi, K., Statistical analysis of extreme auroral electrojet indices, *Earth, Planets Space*, 2015, vol. 67, p. 153. https://doi.org/10.1186/s40623-015-0321-0

Newell, P.T. and Gjerloev, J.W., Evaluation of SuperMAG auroral electrojet indices as indicators of substorms and auroral power, *J. Geophys. Res.*, 2011a, vol. 116, no. A12, p. A12211. https://doi.org/10.1029/2011JA016779

Newell, P.T. and Gjerloev, J.W., Substorm and magnetosphere characteristic scales inferred from the SuperMAG auroral electrojet indices, *J. Geophys. Res.*, 2011b, vol. 116, no. A12, p. A12232. https://doi.org/10.1029/2011JA016936

Nusinov, A.A., Rudneva, N.M., Ginzburg, E.A., and Dremukhina, L.A., Seasonal variations in statistical distributions of geomagnetic activity indices, *Geomagn. Aeron. (Engl. Transl.)*, 2015, vol. 55, no. 4, pp. 493–498. https://doi.org/10.1134/S0016793215040106

O'Brien, P. and McPherron, R.L., Seasonal and diurnal variation of Dst dynamics, *J. Geophys. Res.*, 2002, vol. 107, no. A11, p. 1341. https://doi.org/10.1029/2002JA009435

Ohtani, S. and Gjerloev, J.W., Is the substorm current wedge an ensemble of wedgelets?: Revisit to midlatitude positive bays, *J. Geophys. Res.: Space Phys.*, 2020, vol. 125, no. 9, e2020JA027902. https://doi.org/10.1029/2020JA027902

Rangarajan, G.K. and Iyemori, T., Time variations of geomagnetic activity indices Kp and Ap: An update, *Ann. Geophys.*, 1997, vol. 15, no. 10, pp. 1271–1290. https://doi.org/10.1007/s00585-997-1271-z

Riley, P., On the probability of occurrence of extreme space weather events, *Space Weather*, 2012, vol. 10, no. 2, p. S02012. https://doi.org/10.1029/2011SW000734

Russell, C.T. and McPherron, R.L., Semiannual variation of geomagnetic activity, *J. Geophys. Res.*, 1973, vol. 78, no. A1, pp. 92–108. https://doi.org/10.1029/JA078i001p00092

Sabine, E., On periodical laws discoverable in the mean effects of the larger magnetic disturbances—No. II, *Philos. Trans. R. Soc. London*, 1852, vol. 142, pp. 103–124. https://doi.org/10.1098/rstl.1852.0009

Sergeev, V.A., Angelopoulos, V., Kubyshkina, M., Donovan, E., and Zhou, X.-Z., A. runov a., singer h., mcfadden j., nakamura r. substorm growth and expansion onset as observed with ideal ground-spacecraft themis coverage, *J. Geophys. Res.*, 2011, vol. 116, p. A00I2. https://doi.org/10.1029/2010JA015689

Singh, A.K., Rawat, R., and Pathan, B.M., On the ut and seasonal variations of the standard and SuperMAG auroral electrojet indices, *J. Geophys. Res.: Space Phys.*, 2013, vol. 118, no. 8, pp. 5059–5067. https://doi.org/10.1002/jgra.50488

Svalgaard, L., Cliver, E.W., and Ling, A.G., The semiannual variation of great geomagnetic storms, *Geophys. Res. Lett.*, 2002, vol. 29, no. 16, pp. 12-1–12-4. https://doi.org/10.1029/2001GL014145

Tanskanen, E.I., A comprehensive high-throughput analysis of substorms observed by IMAGE magnetometer network: Years 1993–2003 examined, *J. Geophys. Res.*, 2009, vol. 114, no. A5, p. A05204. https://doi.org/10.1029/2008JA013682

Thomson, A.W.P., Dawson, E.B., and Reay, S.J., Quantifying extreme behavior in geomagnetic activity, *Space Weather*, 2011, vol. 9, no. 10, p. S10001. https://doi.org/10.1029/2011SW000696

Tsubouchi, K. and Omura, Y., Long-term occurrence probabilities of intense geomagnetic storm events, *Space Weather*, 2007, vol. 5, no. 12, p. S12003. https://doi.org/10.1029/2007SW000329

Tsurutani, B.T. and Hajra, R., The interplanetary and magnetospheric causes of geomagnetically inducted currents (GICs) > 10A in the Mäntsälä Finland Pipeline: 1999 through 2019, *J. Space Weather Clim.*, 2021, vol. 11, p. A23. https://doi.org/10.1051/swsc/2021001

Viljanen, A., Tanskanen, E.I., and Pulkkinen, A., Relation between substorm characteristics and rapid temporal variations of the ground magnetic field, *Ann. Geophys.*, 2006, vol. 24, no. 2, pp. 725–733. https://doi.org/10.5194/angeo-24-725-2006

Vorobev, A.V., Pilipenko, V.A., Sakharov, Ya.A., and Selivanov, V.N., Statistical relationships between variations of the geomagnetic field, auroral electrojet, and geomagnetically induced currents, *J. Sol.-Terr. Phys.*, 2019, vol. 5, no. 1, pp. 35–42. https://doi.org/10.12737/stp-51201905

Weibull, W., A statistical distribution function of wide applicability, *J. Appl. Mech.-Trans. ASME*, 1951, vol. 18, no. 3, pp. 293–297.

Werner, R., Guineva, V., Atanassov, A., Bojilova, R., Raykova, L., Valev, D., Lubchich, A., and Despirak, I., Calculation of the horizontal power perturbations of the Earth surface magnetic field, in *Proceedings of the Thirteenth Workshop "Solar Influences on the Magnetosphere, Ionosphere and Atmosphere"*, Primorsko, Bulgaria, 2021, pp. 159–164. https://doi.org/10.31401/WS.2021.proc.

Yanovskii, B.M., *Zemnoi magnetism* (Terrestrial Magnetism), Leningrad: LGU, 1978.

Yermolaev, Y.I., Lodkina, I.G., Nikolaeva, N.S., and Yermolaev, M.Y., Occurrence rate of extreme magnetic storms, *J. Geophys. Res.: Space Phys.*, 2013, vol. 118, no. 8, pp. 4760–4765. https://doi.org/10.1002/jgra.50467

Yoshida, A., Physical meaning of the equinoctial effect for semi-annual variation in geomagnetic activity, *Ann. Geophys.*, 2009, vol. 27, pp. 1909–1914. https://doi.org/10.5194/angeo-27-1909-2009

Translated by A. Ivanov

SPELL: 1. grey